

THE INFLUENCE OF PLATE ANGULAR POSITION IN ITS CROSS SECTION STRESS DISTRIBUTION

Paulo Pedro Kenedi¹

Lucas Lisbôa Vignoli²

¹PPMEM - Programa de Pós-Graduação em Engenharia Mecânica e Tecnologia de Materiais - CEFET/RJ - Av. Maracanã, 229 - Maracanã - RJ - CEP 20271-110 - Brazil

²DEPMC - Departamento de Engenharia Mecânica - CEFET/RJ - Av. Maracanã, 229 - Maracanã - RJ - CEP 20271-110 - Brazil

¹pkenedi@cefet-rj.br

²lucas.lvig@gmail.com

Abstract. Osteosynthesis plates are used to fix broken bones. The plate angular position, that it is fixed at a long bone external surface, can be correlated with forces and moments that are shared with the bone. An analytic model, based in mechanics of solids, is presented to estimate the cross section mechanical plate stress distributions. The result shows the angular position that minimizes the plate stress distribution.

Keywords: osteosynthesis plate; stress analysis; analytic model; long bones; load distribution

1. INTRODUCTION

Human long bones can fracture in different patterns. Figure 1 shows an example bone fracture classification (AO Foundation, 2013). The treatment for these fractures can be carried by different approaches, as: external fixation, intramedullary nailing or osteosynthesis plates (for now one called plate).



Figure 1. Different types of fracture (AO Foundation, 2013).

Plates have been used to fix broken bones, after traumatic occurrences. (Kubiak, 2006) did a review of the history of locked plates and did recommendations for the use of those devices and to look toward future trends in the clinical application of locked plates. Other authors used artificial femurs to tests various types of plates submitted to different types of loads, (Talbot et al., 2008) experimental tested 3rd Generation Composite Femurs in axial, torsional and bending loadings for three plates options: a) lateral locking plate; b) lateral non-locking plate and a medial allograft strut; and c) lateral non-locking plate and intramedullary fibula. The conclusion was that when maximum stiffness is required, the lateral non-locking plate and medial strut should be chosen. (Goswami et al., 2011) did experiments with fourth-generation composite femur, with biomechanical evaluation of LCPs with both locking and non-locking screws (hybrid plating). They concluded that LCPs, constructs secured with locking screws, provide higher axial and torsional rigidity.

Variations of well known procedures were also accessed. (Ahmad et al., 2007) experimental investigate the mechanical stability of a locking compression plate (LCP) construct in a simulated diaphyseal fracture of the humerus at increasing distances between the plate and bone. It was recommended placing the plate at or less than 2 mm from the bone. (Frigg, 2001) has clinical experience with PC-Fix that indicates the advantages of bridging plate osteosynthesis using an internal fixator in comparison to conventional plating procedures.

Although many papers have been written, only a few works discuss plate cross section mechanical stress distribution, most of them using finite element analysis, as in (Kunasek et al., 2012). In this work an analytic approach is used to estimate the angular position influence load distribution between bone and plate. The cross section plate stress distribution resulted from this model can be used to aid to establish an optimized angular position to attach plate to long bones, like a femur, to minimize the occurrence of plate failures.

The simplified analytical model is showed, according to some basic hypothesis of the Solid Mechanics (Crandall, 1978). The femur/plate model, with loads, is illustrated in Figure 2.a (Kenedi, 2012.a). The model considers that plate and bone are placed in parallel arrangement, sharing the load. Stress concentrations, contact forces and screw forces, responsible to fix the plate on bone, are not taking into account.

Figure 2 shows a traditional simplification of a human femur loading forces caused by muscles and the joint reaction force. Also shows a radiographic image and a schematic drawing of side positioned plate on a femur bone.

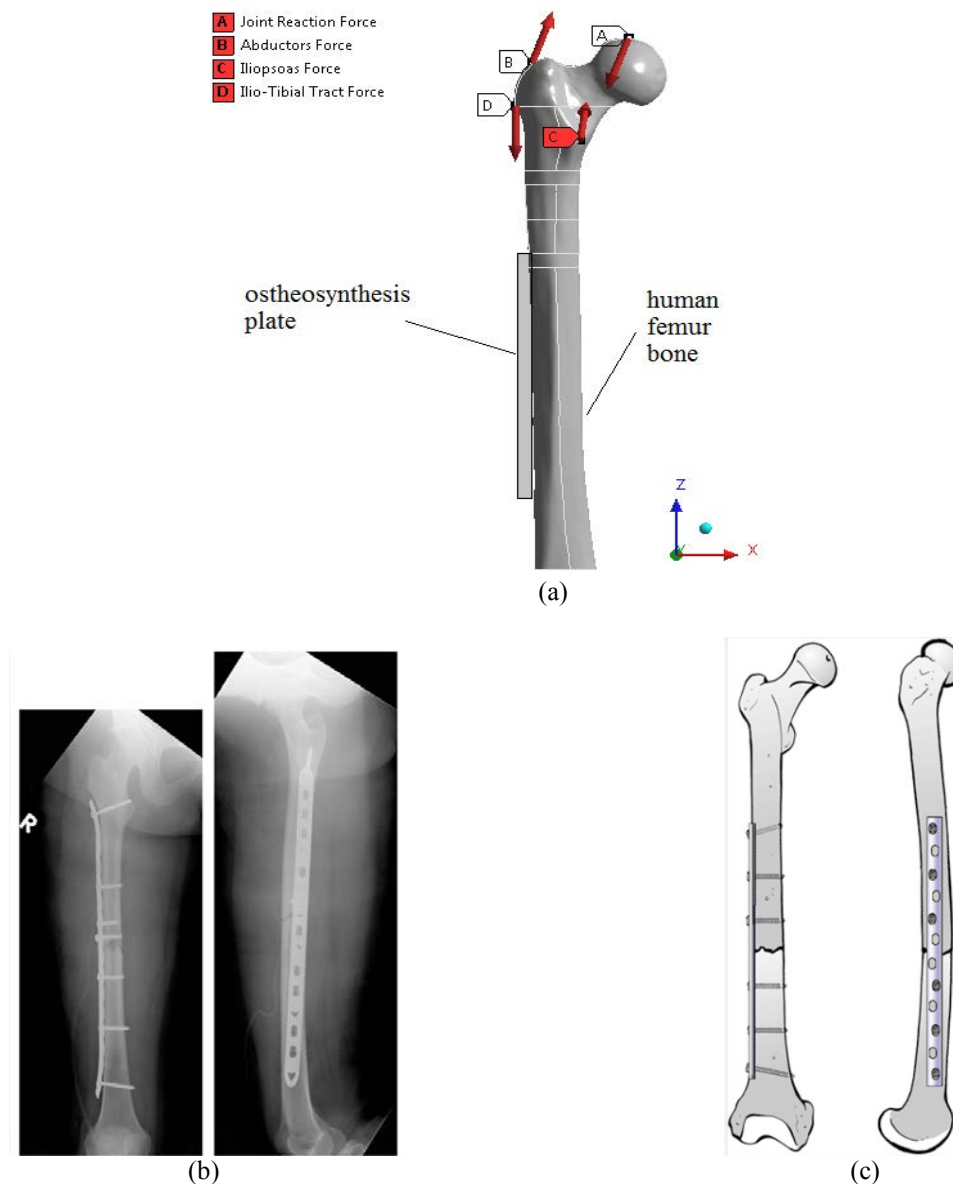


Figure 2. (a) Schematic sketch of a femur load. Femoral plating for a simple fracture pattern: (b) radiographic image and (c) schematic drawing (Rockwood et al., 2006).

2. ANALYTICAL MODEL

A few hypotheses are used to simplify the model construction, for instance, the external loading is represented by four static forces that are concentrated at proximal femur, no bone side ligaments are recognized, the analyzed cross section is medial, the plate shares load with bone, the bone and plate cross sections are assumed to be, respectively, hollow circular and rectangular, no screw holes are analyzed and loads built-in by screws are not recognized. Also the bone tissue is assumed to be cortical and the plate material stainless steel, both modeled as isotropic (Kenedi, 2012.b).

A global and a local coordinates are considered, as showed at Figure 3. The local coordinate axis are attached to cross section centroid and can rotate, in counterclockwise direction, around the femur (x_g positive direction is 0°). Also, figure 3 shows the main cross section dimensions, the analyzed points in plate cross section area (from 0 to 8) and both coordinate systems.

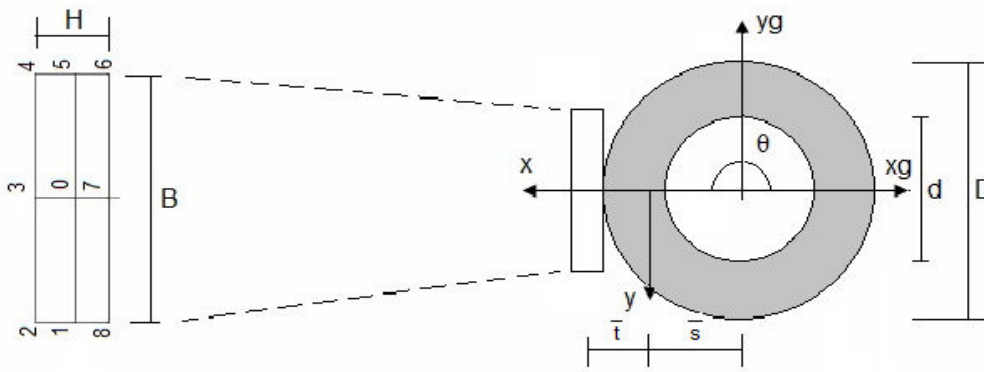


Figure 3. Cross section arrangement for plate at $\theta = 180^\circ$.

Where B and H are, respectively, plate width and thickness, D and d are, respectively bone external and internal diameters. The external forces are named: Joint Reaction force (P_1) at point A, Abductors force (P_2) at point B, Iliopsoas force (P_3) at point C and Ilio-Tibial Tract force (P_4) at point D are schematic shown at Figure 2.

The forces can be written in a vector form, with bold-faced letters, as at (1.a). The distances, from each force to the cross section centroid, can also be written as a vector, at (1.b):

$$\mathbf{P}_i = P_i^{xg} \hat{i} + P_i^{yg} \hat{j} + P_i^{zg} \hat{k} \quad \text{and} \quad \mathbf{d}_i = d_i^{xg} \hat{i} + d_i^{yg} \hat{j} + d_i^{zg} \hat{k} \quad (1)$$

The internal forces and moments, at cross section centroid, written in global coordinates are:

$$\begin{pmatrix} V_i^{xg} \\ V_i^{yg} \\ V_i^{zg} \end{pmatrix} = \begin{pmatrix} P_i^{xg} \\ P_i^{yg} \\ P_i^{zg} \end{pmatrix} \quad \text{and} \quad \begin{pmatrix} M_i^{xg} \\ M_i^{yg} \\ M_i^{zg} \end{pmatrix} = \begin{pmatrix} d_i^{yg} P_i^{zg} - d_i^{zg} P_i^{yg} \\ d_i^{zg} P_i^{xg} - d_i^{xg} P_i^{zg} \\ d_i^{xg} P_i^{yg} - d_i^{yg} P_i^{xg} \end{pmatrix} \quad (2)$$

Where, g subscripts are referenced to global system coordinates. \hat{i} , \hat{j} and \hat{k} are unit vectors. The index i ranges from 1 to 4. The forces and moments components, written in local coordinates, at cross section centroid are:

$$\begin{pmatrix} V_i^x(\theta) \\ V_i^y(\theta) \\ V_i^z(\theta) \end{pmatrix} = \begin{pmatrix} P_i^{xg} \cos(\theta) + P_i^{yg} \sin(\theta) \\ -P_i^{xg} \sin(\theta) + P_i^{yg} \cos(\theta) \\ P_i^{zg} \end{pmatrix} \quad \text{and} \quad \begin{pmatrix} M_i^x(\theta) \\ M_i^y(\theta) \\ M_i^z(\theta) \end{pmatrix} = \begin{pmatrix} M_i^{xg} \cos(\theta) + M_i^{yg} \sin(\theta) \\ -M_i^{xg} \sin(\theta) + M_i^{yg} \cos(\theta) \\ M_i^{zg} \end{pmatrix} \quad (3)$$

To get more compact expressions, some dimensionless constants are established:

$$a^* = \frac{A_p}{A_b} \quad e^* = \frac{E_p}{E_b} \quad g^* = \frac{G_p}{G_b} \quad i_x^* = \frac{\bar{I}_x^p}{\bar{I}_x^b} \quad i_y^* = \frac{I_y^p}{I_y^b} \quad j^* = \frac{J_p}{J_b} \quad (4)$$

Where b and p subscripts refer, respectively to, bone and plate. Also A is area; E is modulus of elasticity; G is shear modulus; J is polar second moment of area. The distance from bone centroid to cross section centroid \bar{s} and from plate centroid to cross section centroid \bar{t} are shown.

$$\bar{s} = \frac{(H + D)/2}{1 + \frac{1}{a^* e^*}} \quad \text{and} \quad \bar{t} = \frac{H + D}{2} - \bar{s} \quad (5)$$

The stresses are estimated by the following expressions:

The plate axial stress σ_{z-N}^p is, (Crandall, 1978):

$$\sigma_{z-N}^p = \frac{N^p}{A_p} \quad (6)$$

where N^p is the plate normal force, defined in Table 1 and A_p is the plate area, defined at Table 2.

The plate bending stresses $\sigma_{z-Mx}^p(\theta)$ and $\sigma_{z-My}^p(\theta)$ are, (Crandall, 1978):

$$\sigma_{z-Mx}^p(\theta) = \frac{M_x^p(\theta)}{\bar{I}_x^p} y \quad \text{and} \quad \sigma_{z-My}^p(\theta) = -\frac{M_y^p(\theta)}{I_y^p} x \quad (7)$$

where $M_x^p(\theta)$ and $M_y^p(\theta)$ are plate bending moments, defined at Table 1 and \bar{I}_x^p and I_y^p , are, respectively, the plate moments of inertia, defined at Table 2. The maximum plate torsional stress τ_{z-T}^p is, (Timoshenko, 1955):

$$\tau_{z-T}^p = \frac{T^p}{BH^2} (3 + 1.8 \frac{H}{B}) \quad (8)$$

where T^p is plate torsional moment, defined at Table 1. The plate transverse shear stresses $\tau_{zx}^p(\theta)$ and $\tau_{zy}^p(\theta)$ are, (Crandall, 1978):

$$\tau_{zx}^p(\theta) = \frac{V_x^p(\theta) Q_y^p(x)}{I_y^p t_y(x)} \quad \bar{t} - \frac{H}{2} \leq x \leq \bar{t} + \frac{H}{2} \quad \text{and} \quad \tau_{zy}^p(\theta) = \frac{V_y^p(\theta) Q_x^p(y)}{I_x^p t_x(y)} \quad -\frac{B}{2} \leq y \leq \frac{B}{2} \quad (9)$$

where $V_x^p(\theta)$ and $V_y^p(\theta)$ are plate transversal forces defined in Table 1. $Q_x^p(y)$ and $Q_y^p(x)$ are plate first moment of area and $t_x(y)$ and $t_y(x)$ are thicknesses, all defined at Table 2.

As the maximum plate torsional stress of (8) is very low, it is neglected. The force and moments components and geometric variables are shown at Appendix. To add the effects of each load in a medial plate cross section, the von Mises criterion $\sigma_{eq}(\theta)$ is applied:

$$\sigma_{eq}(\theta) = \sqrt{(\sigma_{z-N}^p + \sigma_{z-Mx}^p(\theta) + \sigma_{z-My}^p(\theta))^2 + 3((\tau_{zx}^p(\theta))^2 + (\tau_{zy}^p(\theta))^2)} \quad (10)$$

3. RESULTS

These equations were implemented in MathCad and MATLAB software. The geometric dimensions used are: $D=35.6$ mm, $d=22$ mm, $B=16.5$ mm and $H=4.8$ mm. The materials proprieties are: $E_p=190$ GPa, $G_p=73$ GPa, $E_b=20$ GPa, $G_b=8.1$ GPa. The distances (in mm) are: $d_1=(50\cos\theta + 1.1\sin\theta + 11.1, -50\sin\theta + 1.1\cos\theta, 97.5)$, $d_2=(-14.2\cos\theta - 2.6\sin\theta + 11.1, 14.2\sin\theta - 2.6\cos\theta, 79.4)$, $d_3=(-25.3\cos\theta - 0.3\sin\theta + 11.1, 25.3\sin\theta - 0.3\cos\theta, 47.6)$, $d_4=(18\cos\theta - 25.4\sin\theta + 11.1, -18\sin\theta - 25.4\cos\theta, 23.2)$. The loads (in Newton) are: $P_1=(-1062, -130, -2800)$, $P_2=(430, 0, 1160)$, $P_3=(0, 0, -1200)$, $P_4=(78, 560, 525)$ (Bergmann, 2001). Expressions from (1) to (10) were used to generate the graphical results shown at Figure 4. Normal Stress, Shear Stress and von Mises Equivalent Stress distribution are shown at plate nine points cross section area, shown at Figure 3, as a function of angular position θ .

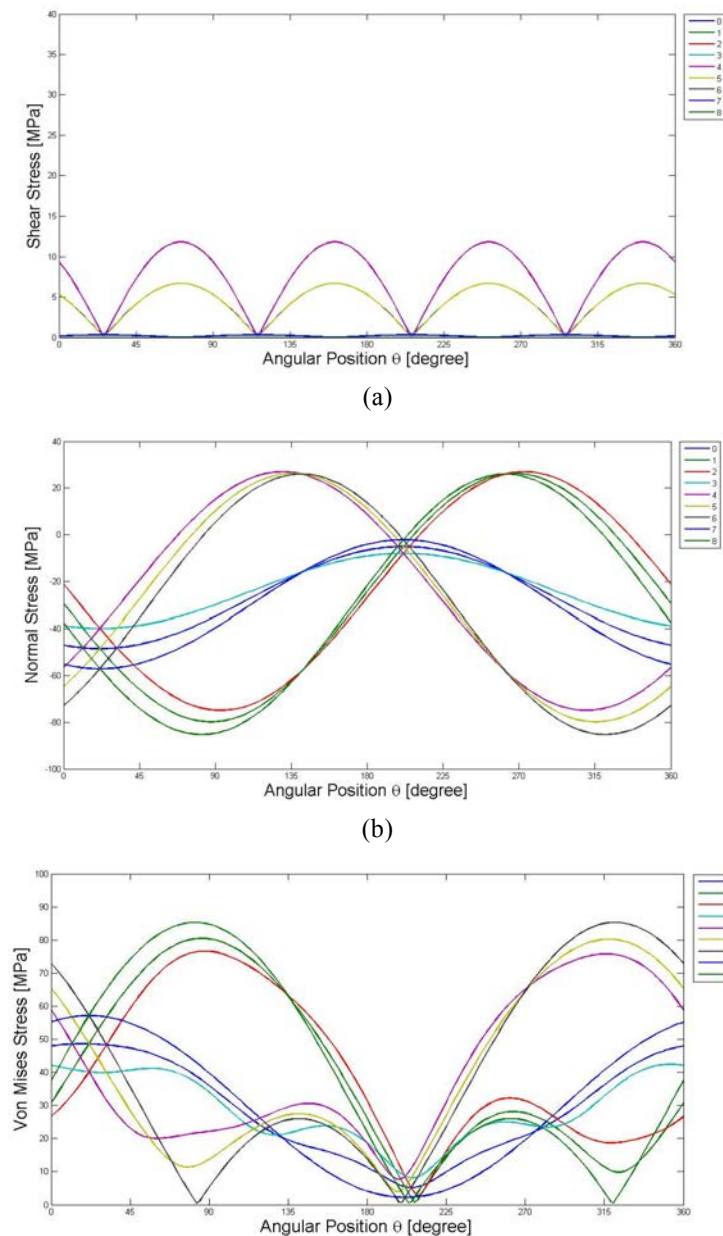


Figure 4. Stress variation with angular position θ : (a)Shear Stress; (b)Normal Stress; (c)von Mises Stress.

Note that the scales of Figures 4.a, 4.b and 4.c are not uniform to emphasize the stress variations in each position. It is possible to recognize that when θ is approximately at 80° , points 1, 2 and 8 have maximum Mises stresses and at 320° , points 4, 5 and 6 have maximum Mises stresses too. Around 200° all nine points have a minimum.

P. P. Kenedi, L. L. Vignoli
The Influence of Plate Angular Position in Its Cross Section Stress Distribution

Figure 5 shows the cross section stress distribution at four different plate angles. Note that the scales not are uniform to emphasize the stress variations in each position.

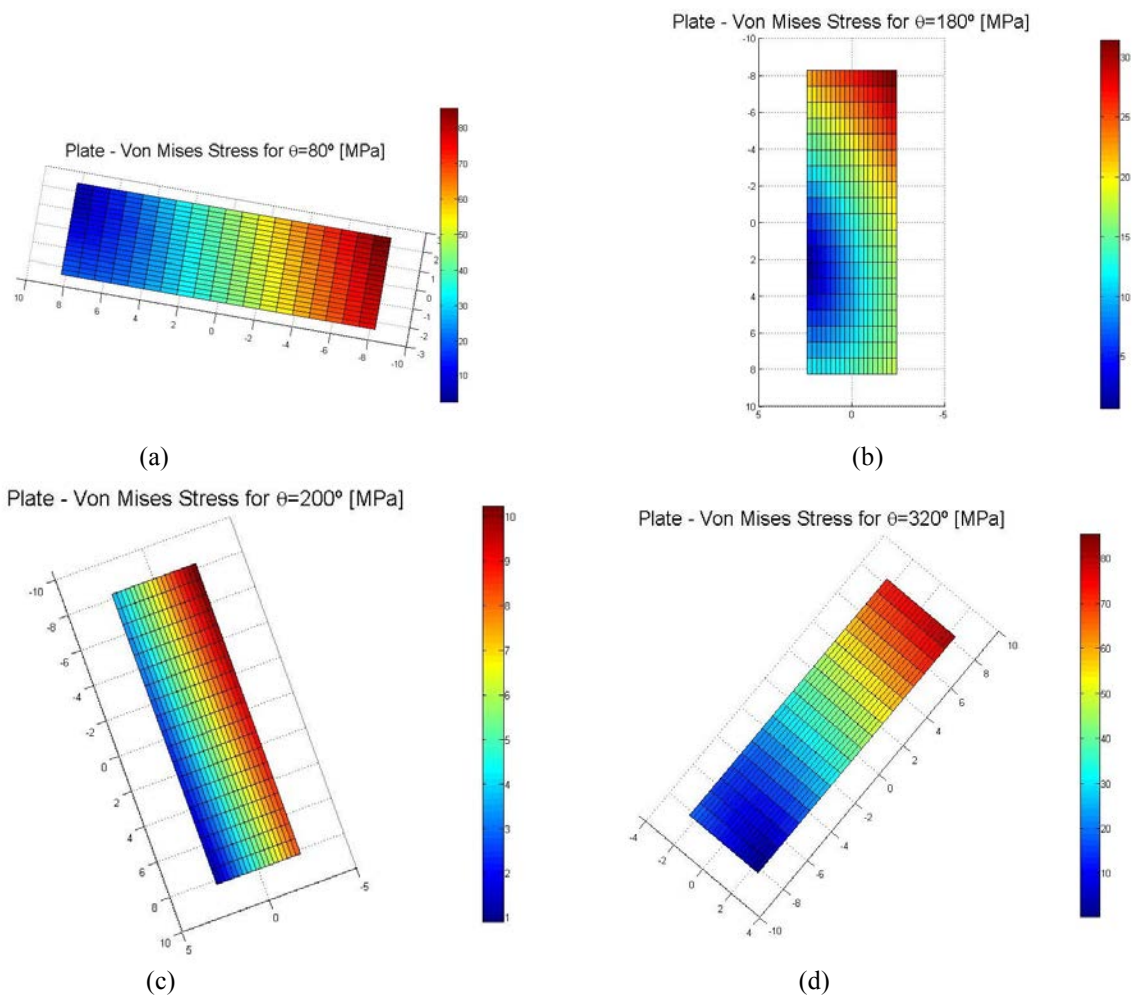


Figure 5. Stress distribution on the plate cross section for angles: (a) $\theta = 80^\circ$, (b) $\theta = 180^\circ$, (c) $\theta = 200^\circ$, (d) $\theta = 320^\circ$.

Figure 6 shows the influence of plate position in cross section plate stress distribution. All the stress distribution are at same scale.

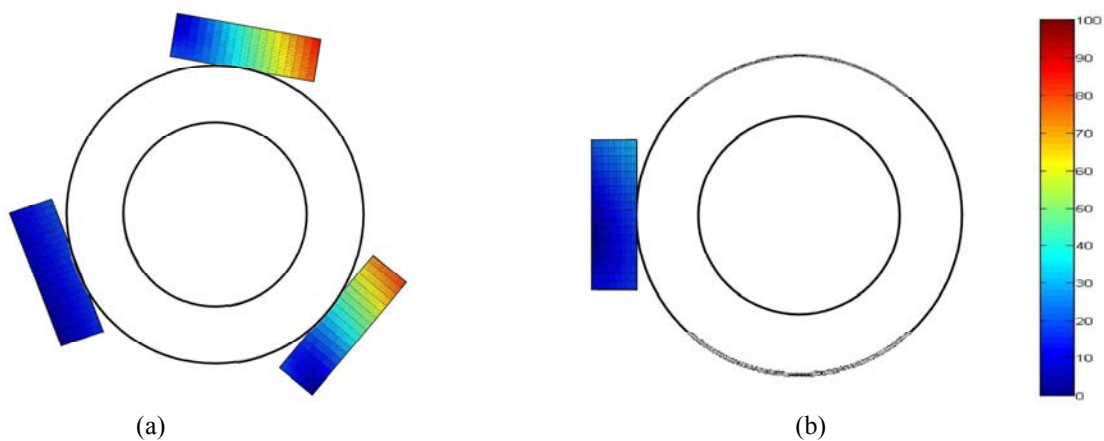


Figure 6: Stress distribution for different plate positions, for (a) $\theta = 80^\circ, 200^\circ$ and 320° and for (b) $\theta = 180^\circ$.

Note that, for the loading adopted in this work (Bergmann, 2001), the better plate angular position is around 200° (Figure 6.a), but at 180° is still a good angular position (Figure 6.b).

4. CONCLUSION

An analytical model, using the concepts of the Mechanics of Solids, was proposed to help to determine the plate optimized position, which have the minimum stress distribution, for a given load condition. It was shown that von Mises stress distribution, in plate cross section, have huge variations in function of plate angular position. As a result of utilization of this analytic model and input data, it was shown that the best angular position to attach a plate at a human femur is around 200°. Also, analyzing von Mises stress distribution, for nine select points, at plate cross section, is clear that the 200° ± 20° range presents also a good performance.

5. REFERENCES

- Ahmad, M., Nanda, R., Bajwa, A.S., Candal-Couto, J., Green, S. and Hui, A.C., 2007, "Biomechanical testing of the locking compression plate: When does the distance between bone and implant significantly reduce construct stability?". *Injury, Int. J. Care Injured*, Vol. 38, p 358-364.
- AO Foundation, 2013, < <https://www2.aofoundation.org/> >.
- Bergmann, G., Deuretzbacher, G., Heller, M., Graichen, F., Rohlmann, A., Strauss, J. and Duda, G.N., 2001, "Hip contact forces and gait patterns from routine activities". *J. Biomech.*, Vol. 34, p 859-871.
- Crandall, S.H., Dahl, N.C., Lardner, T.J., 1978, "An introduction to the Mechanics of Solids", Second Edition with SI units, Mc Graw Hill International Editions.
- Frigg, R., 2001, "Locking Compression Plate (LCP). "An osteosynthesis plate based on the Dynamic Compression Plate and the Point Contact Fixator (PC-Fix)". *Injury, Int. J. Care Injured*, Vol. 32, p SB 63-66.
- Goswami, T., Patel, V. , Dalstrom, D. J. and Prayson, M. J., 2011, "Mechanical evaluation of fourth-generation composite femur hybrid locking plate constructs".
- Karam, L.Z., 2009, "Caracterização de um Fêmur Sintético Empregando o Método dos Elementos Finitos e Validação por Extensometria Ótica". Master Thesis, Universidade Tecnológica Federal do Paraná, Brazil.
- Kenedi, P.P. and Vignoli, L.L., 2013, "Plate Stress Distribution during a Fractured Human Femur Healing Process". *In Proceedings of the 4° National Meeting of Biomechanical Engineering, ENEBI 2013*. Vitória, Brazil.
- Kenedi, P.P., Vignoli, L.L., Furtado, L.A., 2012.b, "Modeling the Loading Share Between an Osteosynthesis Plate and a Human Femur". *In Proceedings of the 7° Congresso Latino Americano de Órgãos Artificiais e Biomateriais, COLAOB 2012*. Natal, Brazil.
- Kenedi, P.P., Vignoli, L.L., Furtado, L.A., Riagusoff, I.I.T., 2012.a, "Osteosynthesis Plate Analytic Model". *In Proceedings of the 7th National Congress of Mechanical Engineering – CONEM 2012*. São Luis, Brazil.
- Kubiak, E. N., Fulkerson, E. S. and Egol, K.A., 2006, "The Evolution of Locked Plates", *J. Bone Joint Surg. Am.* 88:189-200.
- Kunásek, V. and Jírová, J., 2012, "Numerical Analysis of Fractured Femur with Internal Osteosynthesis". *In Proceedings of the 18th International Conference Engineering Mechanics Engineering 2012*. Czech Republic.
- Rockwood and Green, 2006, "Fractures in Adults", Chapter 47 – Fractures of the Shaft of the Femur, Lippincott Williams & Wilkins, 6th Edition.
- Talaia, P.M.D., 2007, "Integridade Estrutural de Placas de Osteossíntese Metálicas e Compósitas para Fixação Óssea". Master thesis, Universidade de Aveiro, Portugal.
- Talbot, M., Zdero, R., Garneau, D., Cole, P.A. and Schemitsch, E.H., 2008, "Fixation of long bone segmental defects: A biomechanical study". *Injury, Int. J. Care Injured*, Vol. 39, p 181-186.
- Taylor, M.E., Tanner, K.E., Freeman, M.A.R., Yettram, A.L., 1996, "Stress and strain distribution within the intact femur: compression or bending?". *Med. Eng. Phys*, Vol. 18, p. 122-131.
- Timoshenko, S., 1955, "Strength of Materials", Third Edition, D. Van Nostrand Company.

P. P. Kenedi, L. L. Vignoli
 The Influence of Plate Angular Position in Its Cross Section Stress Distribution

6. APPENDIX

Tables 1 and 2 shows forces and moments that acts in plate and geometric variables.

$N^p = \left(\frac{1}{1+(a^*e^*)^{-1}} \right) \sum_{i=1}^4 V_i^z$	
$M_x^p(\theta) = \left(\frac{1}{1+(e^*i_x^*)^{-1}} \right) \sum_{i=1}^4 M_i^x(\theta)$	$M_y^p(\theta) = \left(\frac{1}{1+(e^*i_y^*)^{-1}} \right) \sum_{i=1}^4 M_i^y(\theta)$
$V_x^p(\theta) = \left(\frac{1}{1+(e^*i_x^*)^{-1}} \right) \sum_{i=1}^4 V_i^x(\theta)$	$V_y^p(\theta) = \left(\frac{1}{1+(e^*i_y^*)^{-1}} \right) \sum_{i=1}^4 V_i^y(\theta)$
$T^p(\theta) = \left(\frac{1}{1+(g^*j^*)^{-1}} \right) \sum_{i=1}^4 M_i^z(\theta)$	

Table 1: Forces and moments components that acts in plate.

$A_b = \frac{\pi}{4} (D^2 - d^2)$	$A_p = BH$
$\bar{I}_x^b = \frac{\pi}{64} (D^4 - d^4)$	$\bar{I}_x^p = \frac{HB^3}{12}$
$\bar{I}_y^b = \frac{\pi}{64} (D^4 - d^4)$	$\bar{I}_y^p = \frac{H^3B}{12}$
$I_y^b = \bar{I}_y^b + A_b (\bar{s})^2$	$I_y^p = \bar{I}_y^p + A_p (\bar{t})^2$
$Q_x^p(y) = \frac{H}{2} \left[\left(\frac{B}{2} \right)^2 - y^2 \right]$	$Q_y^p(x) = \frac{B}{2} \left[\left(\frac{H}{2} + \bar{t} \right)^2 - x^2 \right]$
$t_x(y) = H$	$t_y(x) = B$
$J_b = \frac{\pi}{32} (D^4 - d^4)$	$J_p = \beta B H^3$

Table 2: Geometric variables.

7. RESPONSIBILITY NOTICE

The authors are the only responsible for the printed material included in this paper.